



# Spatial and temporal characterization of droplet diameter and velocities of a nasal spray atomization

James Van Strien, Sara Vahaji, Petros Lappas, David Morton & Kiao Inthavong

**To cite this article:** James Van Strien, Sara Vahaji, Petros Lappas, David Morton & Kiao Inthavong (2024) Spatial and temporal characterization of droplet diameter and velocities of a nasal spray atomization, *Aerosol Science and Technology*, 58:6, 610-629, DOI: [10.1080/02786826.2024.2332633](https://doi.org/10.1080/02786826.2024.2332633)

**To link to this article:** <https://doi.org/10.1080/02786826.2024.2332633>



© 2024 The Author(s). Published with  
license by Taylor & Francis Group, LLC



Published online: 02 Apr 2024.



Submit your article to this journal



Article views: 345



View related articles



CrossMark

View Crossmark data

# Spatial and temporal characterization of droplet diameter and velocities of a nasal spray atomization

James Van Strien<sup>a</sup> , Sara Vahaji<sup>b</sup>, Petros Lappas<sup>b</sup>, David Morton<sup>a</sup>, and Kiao Inthavong<sup>b</sup> 

<sup>a</sup>School of Engineering, Deakin University, Geelong, Victoria, Australia; <sup>b</sup>Mechanical & Automotive Engineering, School of Engineering, RMIT University, Bundoora, Victoria, Australia

## ABSTRACT

Nasal sprays can deliver drugs topically to the nasal cavity and, alternatively, to the vascular system *via* the nasal epithelium, avoiding painful injections. The atomized spray characteristics can be optimally controlled for the desired parameters such as spray plume, cone angle, droplet velocity and droplet size distribution to target specific locations in the nasal cavity. These parameters have been investigated through computational simulations to evaluate the spray performance within the nasal cavity, however there is a lack of experimental measurements providing three-dimensional velocity data for nasal sprays. This study aims to address key elements of this gap using Phase Doppler Particle Analysis (PDPA) to measure both the droplet size and three-dimensional velocity from two over-the-counter nasal spray devices actuated with a pneumatic device delivering actuation forces equivalent to averaged pediatric, adult, and a maximum adult exertion. In addition to providing experimental data for verifying CFD simulations, this study provides multiple, and some unique, presentations of characterizing the nasal spray velocity and size behavior. Multiple new conclusions were drawn from this study, including a demonstration that the spray droplet axial velocity is the dominant velocity component, followed by radial velocity. Tangential velocity exists but is negligible by comparison. Finer droplets tended to move slower and were predominantly found in the spray core (although this may not be the case with a fluid of higher viscosity). Larger, faster droplets are found near the spray's edge in the pressure-swirl nasal sprays. The mean resultant velocity between both devices at 15 mm from the nozzle tip, actuated at the mean adult force was 16.9 m/s. The mean  $D_{32}$  and  $D_{v50}$  of both devices at the mean adult actuation force was 23.0  $\mu\text{m}$  and 80.0  $\mu\text{m}$ , respectively.

## ARTICLE HISTORY

Received 25 October 2023

Accepted 26 February 2024

## EDITOR

Darragh Murnane

## 1. Introduction

Nasal sprays can deliver drugs systemically by exploiting the highly vascularized mucosa. Insight into nasal spray characteristics is needed to achieve deposition to targeted locations of the nasal cavity to reach the full potential of nasal drug delivery. Spray characteristics such as cone angle, dispersion angle, break-up length and droplet size are available in the literature for nasal sprays. However, limited data are available for droplet velocity, despite it being a contributing factor to deposition within the nasal cavity (Inthavong et al. 2006; Kimbell et al. 2007; Gao, Shen, and Mao 2020). Phase Doppler Anemometry, also known as Phase Doppler Particle Analysis (PDA or PDPA) is a method of measuring droplet size and velocity in a small volume using laser interferometry, where

laser beam pairs intersect. PDPA use is popular amongst the literature for high-pressure, high-flow nozzle applications (Belhadeff et al. 2012; Sumer et al. 2012; Dorfner et al. 1995; Dafsari et al. 2019b; Durdina, Jedelsky, and Jicha 2014; Tratnig and Brenn 2010; Zhao and Yang 2012; Durdina, Jedelsky, and Jicha 2012; Sun et al. 2018; Dafsari, Vashahi, and Lee 2017; Hansen et al. 2002; Dafsari et al. 2019a). These studies apply to nozzles of similar design to nasal sprays but on a larger and industrial scale in terms of geometry, fluid pressure and flow rate, and therefore the findings may not apply to smaller devices.

While the bulk of PDPA studies are used in combustion applications, there are a few studies related to nasal sprays. Liu, Doub, and Guo (2010), measured

**CONTACT** Kiao Inthavong  [kiao.inthavong@rmit.edu.au](mailto:kiao.inthavong@rmit.edu.au)  Mechanical & Automotive Engineering, School of Engineering, RMIT University, Bundoora, Victoria, 3083, Australia.

© 2024 The Author(s). Published with license by Taylor & Francis Group, LLC  
This is an Open Access article distributed under the terms of the Creative Commons Attribution-NonCommercial-NoDerivatives License (<http://creativecommons.org/licenses/by-nc-nd/4.0/>), which permits non-commercial re-use, distribution, and reproduction in any medium, provided the original work is properly cited, and is not altered, transformed, or built upon in any way. The terms on which this article has been published allow the posting of the Accepted Manuscript in a repository by the author(s) or with their consent.

droplet size and velocity from three nasal spray devices, concluding that nasal sprays can be characterized by measurements on or near the concentric centerline of the nozzle, where the spray plume has the highest particle count. Pump A had average velocities of  $7.3 \text{ m/s}$  to  $12.2 \text{ m/s}$ , pump B varied between  $4.9 \text{ m/s}$  to  $11.5 \text{ m/s}$  and pump C  $1.8 \text{ m/s}$  to  $11.3 \text{ m/s}$ , the variations of which depended on the measurement location. Later, Liu, Doub, and Guo (2011) repeated the measurements for seven different nasal sprays to investigate the influences of stroke length, actuation velocity, viscosity (with the addition of a gelling agent) and surface tension (with the addition of a surfactant) on droplet velocity and size. The authors concluded that all four factors influenced droplet velocity, providing an optimized quadratic model to quantify the influence of stroke length, actuation velocity, viscosity and surface tension on droplet velocity. The range of mean droplet velocities varied from  $8.91 \text{ m/s}$  to  $17.56 \text{ m/s}$ . Hosseini et al. (2019) provided velocity data of three nasal drug delivery devices using PDPA with high-speed videography, finding an average velocity of approximately  $14.5 \text{ m/s}$ . These are the only three examples of PDPA studies of nasal sprays found in the literature. While each of these studies provides important information, a limitation to all three is that they only capture axial velocity, while in reality, individual droplets exhibit three-dimensional velocity components.

Some studies have used Particle Image Velocimetry (PIV) to investigate nasal spray performance, where PIV is a technique for measuring flow field velocity. It uses a high-speed camera with a double-pulsed laser sheet that illuminates seeded tracer particles in a thin plane of interest. The time between pulses of the laser sheet and the distance per pixel are known, allowing velocities to be determined by comparing two sequential images taken during each laser pulse. When using PIV to measure droplet velocity from a spray device, the droplets themselves act as the seeding particles. Inthavong et al. (2012) used PIV to derive the spray velocity, and a droplet image analysis to determine the spray cone angle and droplet size of a continuously flowing nasal spray. They concluded that droplet sizes varied at different downstream spray locations. The PIV and image analysis method was repeated in later studies using an automated actuation device, concluding that an increase in actuation force causes an increase in droplet velocity and a decrease in droplet size (Inthavong et al. 2014). By measuring the actuation displacement of the nozzle, they also provided a displacement profile which was related to

actuation force, droplet size and droplet velocity (Inthavong et al. 2015). Williams, Gilles, and Murphy (2009) provided mean and maximum droplet velocities from three nasal sprays using PIV, however, they do not specify the planes in which they take their measurements. At most, these four PIV studies investigate spray velocity in two dimensions, missing the velocity component in the third direction.

This paper provides an experimental method to acquire three dimensional droplet velocity profiles from two commercially available nasal sprays, which have not been reported before.

## 2. Method and materials

Measurements of droplet size and velocity from atomized spray through two different nasal sprays were acquired using PDPA.

### 2.1. Nasal sprays devices

Flixonase anti-inflammatory and Mendeleev nasal decongestant bottles were chosen for this study as they are available over-the-counter devices. Both the devices are “pressure-swirl atomizers,” where tangential velocity is imposed on the fluid before exiting the nozzle, which causes the fluid to form a thin liquid sheet hollow cone with an air core as it exits the outlet orifice. The hollow cone generates shearing forces with the surrounding gas, causing perturbations. These disturbances cause localized thinning of the liquid sheet, causing liquid “ligaments” to detach from the cone sheet. These long stretches of liquid ligaments continue to break up into droplets (Lefebvre and McDonell 2017).

The drug formulations were removed from the nasal spray devices and replaced with water, as water is safe to use and many spray events were recorded. The fluid properties of water are well-known and it allowed a consistent comparison between two devices independent of the working fluid. Drug formulations are typically of a higher viscosity than water, which impacts droplet size distribution (Dayal, Sudhan Shaik, and Singh 2004) and droplet velocity (Liu, Doub, and Guo 2011). Nasal sprays may also contain surface tension modifiers, but Guo et al. (2008) found this had the least impact on nasal spray behavior when compared to viscosity, actuation stroke length and actuation velocity. With these influencing factors acknowledged, water is an acceptable surrogate to demonstrate the novel technique for measurement of

three-dimensional droplet velocity and provide examples of potential insights into nasal spray behavior.

## 2.2. Actuation device

A pneumatic actuator system was used to apply consistent and repeatable actuation to the nasal spray devices, at forces representing an average child, average adult and an adult using maximum exertion of 31, 63, and 94 N, respectively (Doughty et al. 2011). The details of the actuation system are further explained in previous works (Van Strien et al. 2022).

## 2.3. PDPA

Droplet size and velocity were captured with a three-channel TSI PDPA system and a Spectraphysics Stabilite 2017 argon-ion laser. The system was controlled by the TSI FlowSizer software and was able to measure droplet sizes in the range of 0.58  $\mu\text{m}$  to 200  $\mu\text{m}$ . Multiple locations were measured within the spray plume as the PDPA is a point measuring device, where the probe volume is a fraction of a millimeter in diameter. A photo and schematic of the PDPA

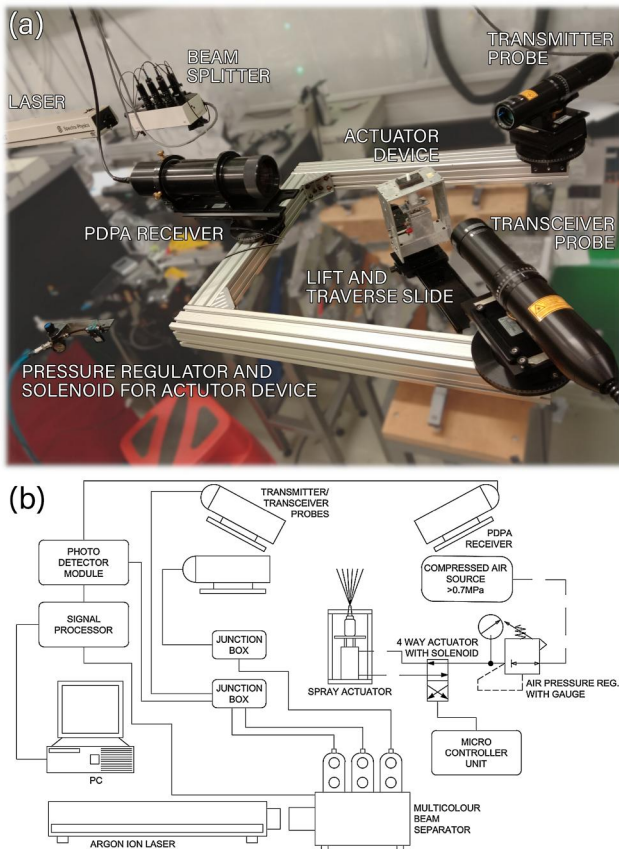


**Figure 1.** Photo and schematic images detailing the PDPA setup. (a) Photo of the equipment in the lab. (b) Schematic of the experimental setup.

system are given in [Figure 1](#). The actuator system was mounted to a platform with a small scissor jack, allowing measurements at heights of 15, 30, and 60 mm from the nozzle tip. This jack was mounted to a traverse device with millimeter markings and aligned with the channel 1 probe measuring axial droplet velocity and diameter. The measurements were taken at multiple radial distances; every 2 mm radially at heights of 15 mm and 30 mm, and every 4 mm radially at a height of 60 mm ([Figure 2](#)). For each location, 6–10 spray events were recorded. The zero height reference was found by running the laser at a very low wattage and moving the nozzle tip until it touched the probe volume. The HVAC system in the lab was turned off during measurements to prevent airflow from influencing the results. Fluid tends to pool at the nozzle tip after repeat actuations which causes large ligaments to form during the spray. This is not typical of a use case. Fung et al. (2013) used absorbent media to remove pooling between spray

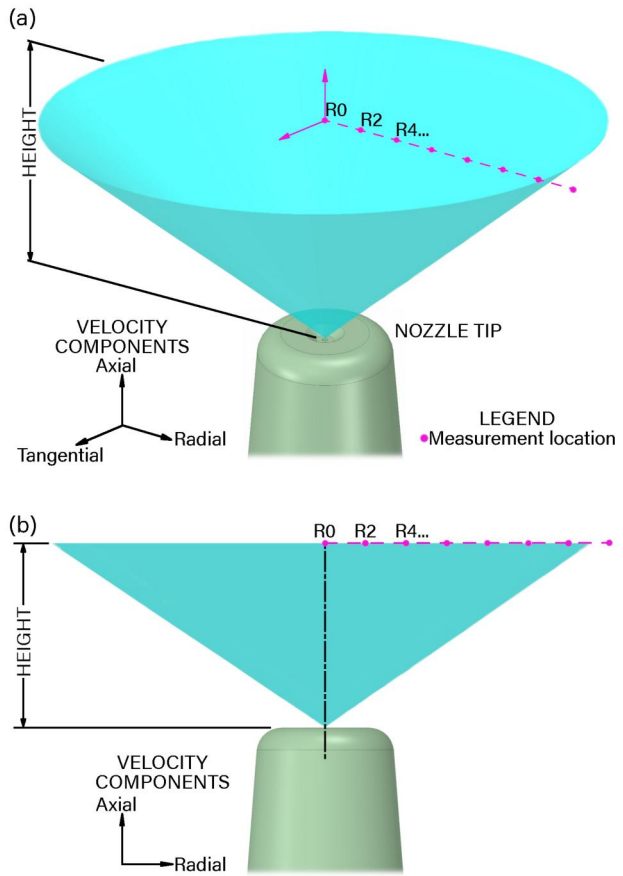


**Figure 2.** Coordinate system and measurement locations relative to the nozzle tip. (a) Isometric view; (b) front view. R0 indicates the location directly above the nozzle tip, while R2 is 2 mm distance in the radial direction from the center. The height distances measured from the nozzle tip were 15, 30, and 60 mm.

events, but still found additional ligaments. Compressed air was used between sprays to clear the nozzle tip of pooling, as per previous work (Van Strien et al. 2022).

#### 2.4. Data processing

The nasal sprays were operated vertically upwards. Erroneous data were found in the form of falling droplets as the sequential sprays were continuously recorded. These erroneous data were removed by determining the droplets that were 0.1 s or more out of the duration time of each spray event. Partially recorded sprays (when the PDPA system stopped or started recording during a spray event) were also removed from the data. A comparison of a scatter plot from the original unfiltered data with the filtered data allowed the authors to ensure that only the invalid data were removed.

#### 2.5. Actuation filming

A video camera was used to film the actuation device and nasal spray cone of the spray bottles at each actuation force, to compare the timing between the end of actuation stroke and the collapse of the spray cone (indicating end of spray). The purpose of this investigation was to find evidence of stored fluid pressure in the nasal spray devices. If there is a significant delay between the end of stroke and the end of the spray event, then fluid pressure must be stored during actuation. The camera was set to record at 240 frames per second, approximately 4.2 ms between frames. Each actuation force was filmed 4 times, thereby producing 12 recorded spray events per bottle. Any delay between the end of the actuation stroke and the end

of spray was determined through manually processing incremental video frames, shown in Figure 3.

### 3. Results and discussion

The point-measurement nature of the PDPA system provides measurements of the droplet velocity and sizing at precise locations within a spray plume. All  $3 \times 3$  subplots in this paper are arranged whereby columns are grouped by actuation forces, 31, 63, and 94 N from left to right and rows are grouped by distance from the nozzle tip, 15, 30, and 60 mm from bottom to top.

#### 3.1. Tables of size and velocity

The data collected in this study are presented in multiple formats. A table for droplet size is presented for each spray nozzle at each actuation force in Table 1. These data were measured at radial locations at a height of 15 mm from the nozzle tip. "Count" refers to the number of data points.  $D_{32}$  is the Sauter Mean Diameter (SMD), which is the diameter of a spherical particle that has the same volume-to-surface area ratio as the sampled spray (Kowalcuk and Drzymala 2016). It provides insight into the general fineness of a spray; a lower  $D_{32}$  indicates a larger proportion of smaller droplets. The SMD is calculated by first finding the Sauter diameter,  $d_{32}$ , for each droplet:

$$d_{32} = 6 \frac{V_d}{A_d}$$

where  $V_d$  and  $A_d$  are the volume and surface area of the droplet, respectively. The Sauter mean diameter,  $D_{32}$ , is then the mean of all  $d_{32}$  values. Note these values were calculated assuming spherical droplets.  $Dv_{10}$ ,  $Dv_{50}$ , and  $Dv_{90}$  are the sizes below which the

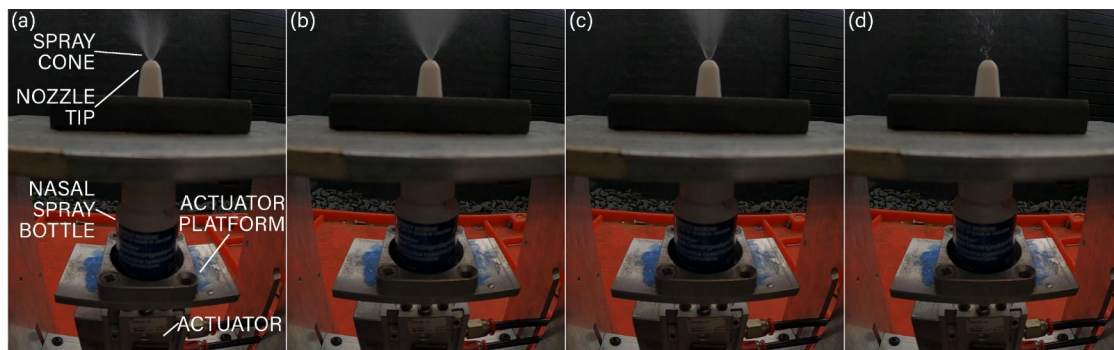


**Figure 3.** Selected video frames (side and oblique views) of the Mendeleev bottle actuated at 94 N. Video frame (a) when the actuator starts moving and the fluid begins spraying; (b) when the actuator platform has stopped moving yet the spray cone continues; (c) where the fluid continues dispensing from the nozzle which was 8 frames (33 milliseconds) after video frame in (b); and (d) of the spray cone which ends in the next frame.

**Table 1.** Tabulated results of droplet size at a distance of 15 mm from the nozzle tip, all radial locations.

Spray device	Actuation force [N]	Count	Droplet diameter [ $\mu\text{m}$ ]					
			$D_{32}$	$Dv_{10}$	$Dv_{50}$	$Dv_{90}$	Min	Max
Flixonase	31	12401	21.77	44.34	85.72	134.97	0.58	184.25
	63	13267	22.12	41.11	77.90	124.89	0.58	173.39
	94	15514	14.59	32.88	64.50	119.13	0.58	195.86
Mendeleev	31	12213	23.78	42.40	80.13	127.28	0.59	191.25
	63	10668	23.93	43.14	82.03	132.30	0.59	193.37
	94	10932	22.80	40.26	78.33	132.03	0.59	179.76

See Figure 2 for measurement locations. Note that "Count" is the number of droplets measured and  $D_{32}$  is the Sauter mean diameter. Data processed as described in Section 2.4.

**Table 2.** Tabulated results of droplet velocities at a distance of 15 mm from the nozzle tip, all radial locations.

Spray device	Actuation force [N]	Axial Droplet Velocity [m/s]					Radial Droplet Velocity [m/s]					Tangential Droplet Velocity [m/s]				
		Mean	SD	Min	Median	Max	Mean	SD	Min	Median	Max	Mean	SD	Min	Median	Max
Flixonase	31	11.89	4.83	-0.67	11.03	37.48	1.16	1.80	-3.61	0.75	8.80	-0.67	1.01	-5.53	-0.65	8.62
	63	16.49	6.61	-0.82	14.92	41.45	5.90	3.55	-3.05	6.51	17.28	-1.33	1.14	-9.23	-1.38	7.71
	94	19.82	6.74	-0.91	18.90	49.65	9.35	5.24	-3.37	10.65	21.01	-1.47	1.07	-6.00	-1.51	3.14
Mendeleev	31	10.84	5.01	-0.20	9.81	30.85	3.51	3.22	-4.76	3.01	22.80	-0.08	1.22	-4.99	0.07	3.81
	63	14.34	7.31	-0.48	12.67	41.86	7.64	6.26	-4.05	6.61	23.62	-0.32	1.37	-8.64	-0.14	4.02
	94	16.08	8.65	-0.36	14.31	49.18	10.68	8.20	-3.97	10.18	29.04	-0.34	1.39	-6.61	-0.21	10.66

See Figure 2 for velocity and measurement locations. SD is the standard deviation of the data set. Data processed as described in Section 2.4.

cumulative total volume of the spray is 10%, 50%, and 90%, respectively. "Min" and "Max" are the minimum and maximum droplet diameters recorded.

The SMD produced by the Mendeleev device was less influenced by actuation force than the Flixonase device (referring to Table 1), where a variation of  $1.13\mu\text{m}$  was found between the 94 N to 31 N actuation force for the Mendeleev device, while the Flixonase  $D_{32}$  varied by  $7.53\mu\text{m}$ . The range for  $Dv_{10}$ ,  $Dv_{50}$ , and  $Dv_{90}$  for Mendeleev was  $2.88\mu\text{m}$ ,  $3.70\mu\text{m}$ , and  $5.02\mu\text{m}$ , while for Flixonase it was  $11.46\mu\text{m}$ ,  $21.22\mu\text{m}$ , and  $15.84\mu\text{m}$ , respectively.

Tabulated velocity data for each nozzle at each actuation force at 15 mm from the nozzle tip is given in Table 2. This includes the mean, standard deviation, minimum, median and maximum velocities of each direction; axial, radial and tangential (see Figure 2 for definitions of velocity directions). Due to the fixed-volume nature of the nasal spray pump, it would be expected that an increase in actuation force would result in an increase in droplet velocity. This is reflected for both axial and radial velocities in Table 2 where the mean, median and maximum values increase with an increase in actuation force. It was presumed that tangential velocity would average to zero, as the authors believe the tangential velocity component within the nozzle swirl chamber is transferred to radial velocity (based on mass conservation) once it has left the outlet orifice, creating the cone shape. While the mean and median tangential velocities of both spray devices are small, potential source for the non-zero values is simply the chaotic nature of

the spray; eddies of air within the spray cause some tangential velocity. Another possible cause may be a slight misalignment between the nozzle center and the probe volume of the PDPA system. An investigation of pressure-swirl atomizers for aircraft combustion engines by Durdina, Jedelsky, and Jicha (2014) found that tangential velocity was negligible in comparison to axial velocity and approached zero downstream of the nozzle. While the pressure, geometry and flowrate are much greater in combustion applications, their conclusion is consistent with our interpretation of our data.

### 3.2. Size distribution histograms

Histograms showing droplet diameter size distributions by number count for each nasal spray are presented in Figure 4, with bin sizing of  $1\mu\text{m}$ . The top  $3 \times 3$  subplots are for the Flixonase device and the bottom  $3 \times 3$  subplots are for the Mendeleev. Each subplot represents data at all measured radial locations per height plane. Typically, it can be seen the diameter count is the highest at the  $30\text{ mm}$  plane, second highest at the closer  $15\text{ mm}$  plane (as there are approximately half as many radial locations to measure) and least at the  $60\text{ mm}$  plane where the spray plume density decreases.

Droplet size distribution (DSD) is presented in two forms throughout the figures in this study; count and percent of total volume. The PDPA system measures in terms of count and is included as it allows an additional means for data comparison and indicates how much data are acquired. Because this study involves

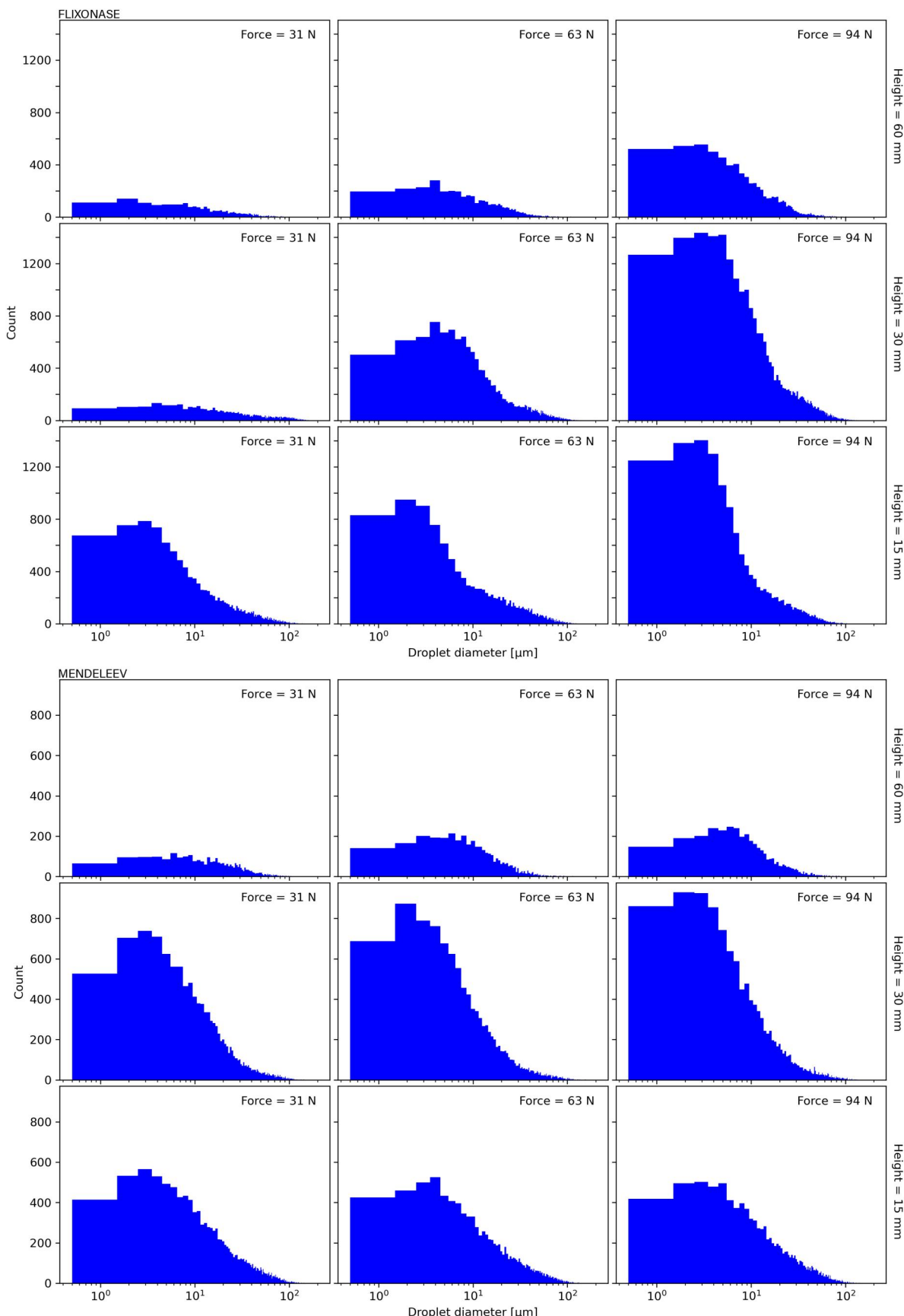


**Figure 4.** Histogram of droplet diameter count with bin sizing of  $1\mu\text{m}$  and log x-axis. TOP: Flixonase, BOTTOM: Mendelev, 3x3 subplots. Columns depict actuation force and rows are height from nozzle tip. Sizing data taken from all radial locations at given height. Data processed as described in Section 2.4. See Figure 2 for measurement locations.

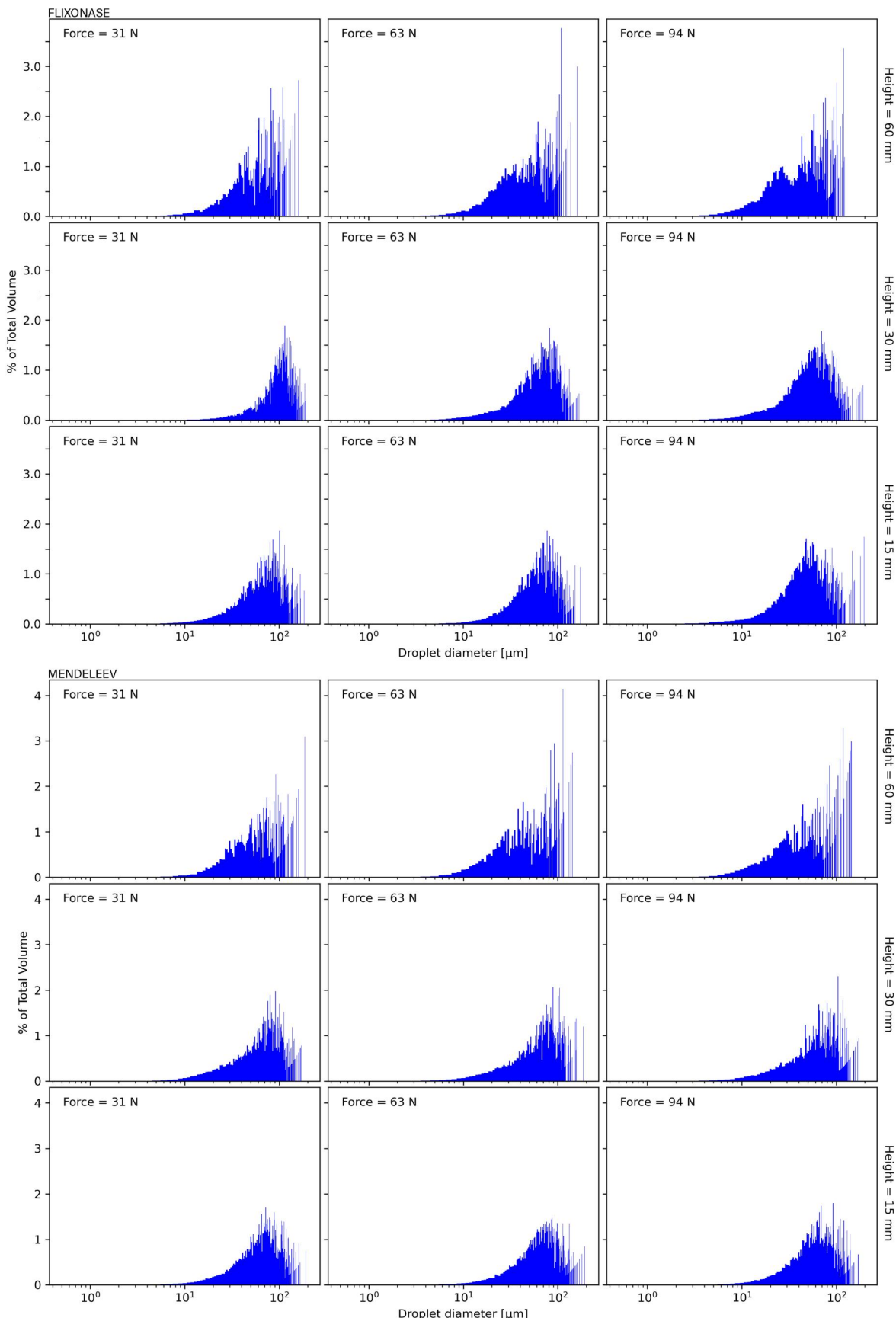


**Figure 5.** Histogram of droplet diameter as a percentage of total volume of spray with bin sizing of  $1 \mu\text{m}$  and log x-axis. TOP: Flixonase, BOTTOM: Mendeleev, 3x3 subplots. Columns depict actuation force and rows are height from nozzle tip. Sizing data taken from all radial locations at given height. Data processed as described in Section 2.4. See Figure 2 for measurement locations.

drug delivery mechanisms, the percent of total volume is also included as it is a preferred metric for such devices that represents dose delivery. [Figure 5](#) provides additional histograms in the same layout as [Figure 4](#), again with  $1 \mu\text{m}$  bin sizing but as a percent of total volume. Comparing these two sets of histograms shows a distinction between count and volume fraction when presenting DSD, where the distributions skew in opposite directions. [Figure 4](#) indicates large quantities of smaller droplets in the  $0.5 \mu\text{m}$  to  $8 \mu\text{m}$  droplet diameter range, while [Figure 5](#) shows the bulk of the droplets by volume are found in the  $50 \mu\text{m}$  to  $100 \mu\text{m}$  range.

[Figure 6](#) provides a direct comparison between DSD data from the present study (using PDPA) and previous work (Van Strien et al. 2022) utilizing the laser diffraction method. The nozzle and pump devices, actuation forces and heights from nozzle tip are all the same. The laser diffraction method data measured the drug DSD, while the present study measured water. The viscosity of nasal sprays are usually higher than water to reduce the amount of smaller droplets, to decrease the amount of drug deposition beyond the nasal cavity. The laser diffraction data (drug) generally indicates a larger portion of smaller droplets compared to the present study (water) but this can be explained by the work of Sijs et al. (2021), who found that the laser diffraction method overestimated the amount of smaller droplets due to the large measurement volume being averaged over time and smaller droplets having less velocity. With this in mind, we find the matching shapes of our present data to be an indication of its validity.

[Figure 7](#) show histograms of droplet size distribution with different actuation forces overlayed where each row of subplots represents the measured height from the nozzle tip ( $60$ ,  $30$ , and  $15 \text{ mm}$ ), and the columns are for the Flixonase and Mendeleev devices. The DSD behavior by droplet count for the Flixonase device showed that increased actuation force produced a greater quantity of smaller droplets, which is expected since greater actuation force provides more energy imparted onto the fluid for break-up. The Mendeleev device behaved a little differently. At  $60 \text{ mm}$  and  $30 \text{ mm}$  heights, the DSD profiles exhibited a similar trend with peak droplet sizes around  $1 \mu\text{m}$  to  $10 \mu\text{m}$  range. At a height of  $15 \text{ mm}$ , the DSD were invariant for all three actuation forces.

The DSD behavior by volume fraction ([Figure 7b](#)) showed similar trends where the Flixonase device produced finer droplets with increased actuation force, while the DSD produced from the Mendeleev device

was very much independent of the actuation force. There is a shift to the right in the peak or median size of the DSD when looking at the percentage of droplets by volume fraction, compared to the DSD by droplet count, implying the volume equivalent mean diameter is much larger than the mean diameter by droplet count.

### 3.3. Boxplots of velocity

Boxplots of axial and radial velocities are shown in [Figures 8](#) and [9](#) for Flixonase and Mendeleev, respectively. Refer to [Figure 2](#) for a diagram of measurement locations. Due to the conical spray plume, the axial and radial velocities vary at different radial locations.

The axial velocity exhibits an inconsistent profile for both devices, heights and actuation forces; however, a general pattern of faster velocities is found near the center ( $r = 0 \text{ mm}$ ), which then slows down slightly out from the center and then increases in velocity near the outer spray peripheral edge. This can be explained by the swirling sheet breaking into a hollow cone of droplets that form where the thin conical sheet was. Larger droplets that form contain greater momentum and move along the outer spray cone but the chaotic airflow within the spray causes smaller droplets to move closer to the center.

For the radial velocity component, the velocity is close to zero at the center ( $r = 0 \text{ mm}$ ), which is directly above the nozzle orifice, and increases further from the center. This tendency is a result of the conical shape of the spray plume. There is a decrease in radial velocity at some of the outer peripheral locations, as these measurements were taken on the fringes of the spray cone.

Boxplots of tangential velocity are given in [Figure 10](#). The tangential velocity component was negligible as the swirling motion from within the nozzle was transferred to radial velocity as the spray leaves the orifice. While the boxplots of tangential velocity ([Figure 10](#)) include non-zero values, this is attributed to the chaotic nature of the spray producing fluctuations and that there is no true tangential component to the droplets. The biased means of tangential velocity are likely due to imperfect alignment of the traverse system or possibly due to the asymmetrical nature of spray plumes.

### 3.4. Diameter – velocity scatterplots

An advantage to the PDPA system used in this study is that it simultaneously measures axial velocity and

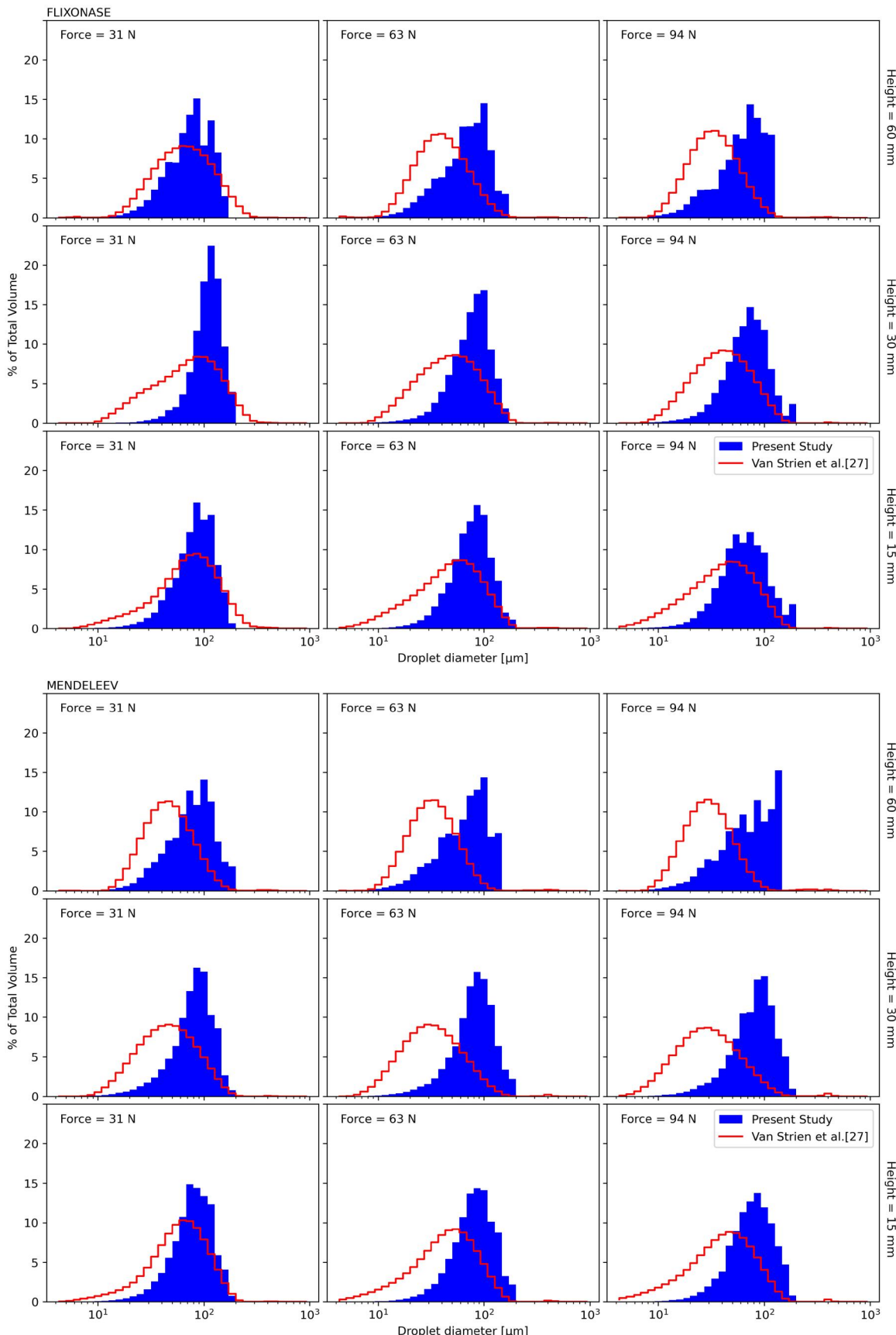


**Figure 6.** Comparison of droplet size distribution measurements from present study (blue, using PDPA) and a previous study (red, using the laser diffraction method). Bin sizing is logarithmic and equal for both data sets. The earlier study used the drug from each product while present study used water.

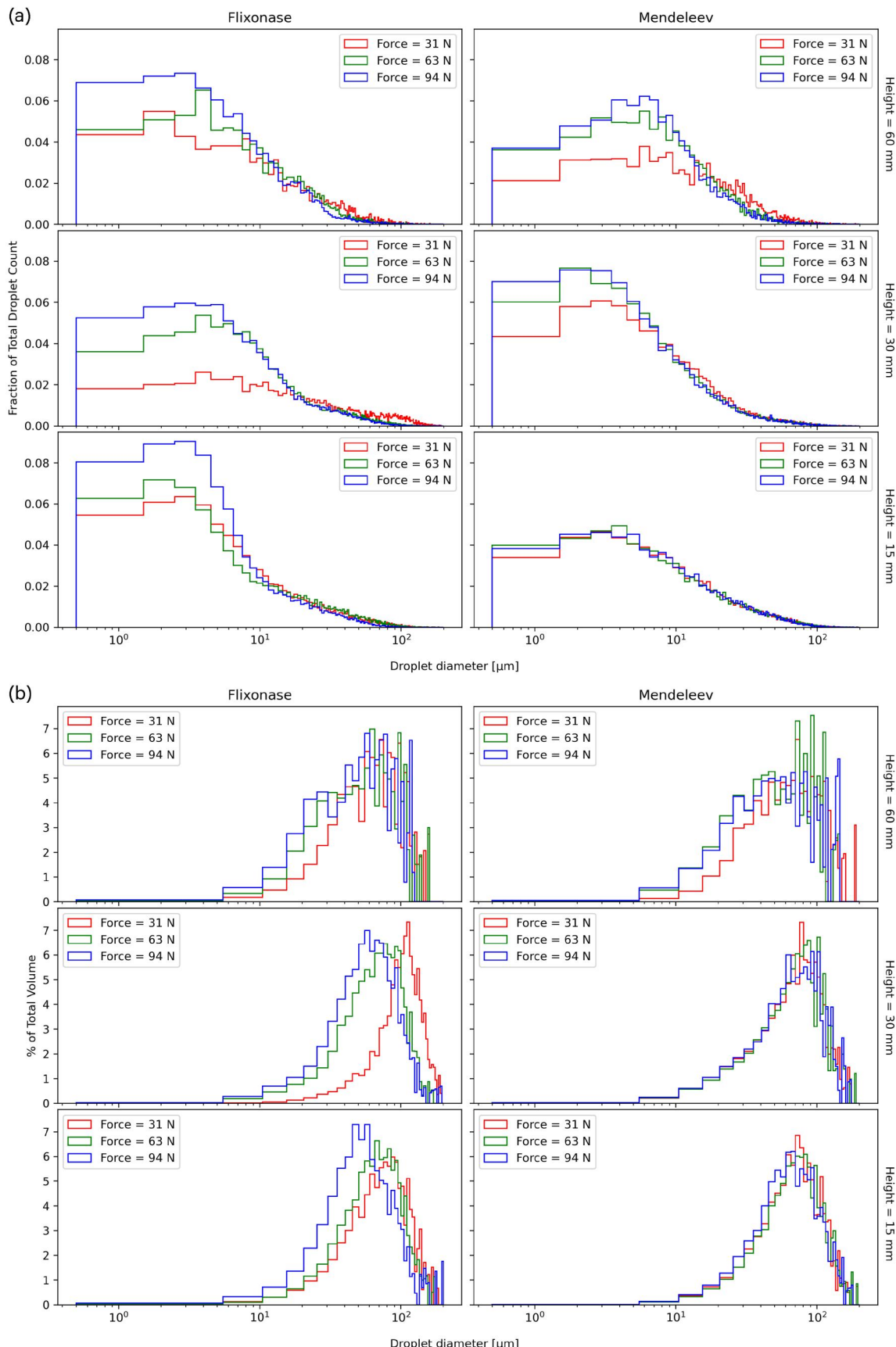


**Figure 7.** Histograms of droplet diameter (on a log x-axis), grouped by actuation forces where each row is a different height from the nozzle tip. The left column is for the Flixonase device, right column for Mendeleev. (a) With the y-axis presenting the fraction of the total droplet count with bin sizing of  $1 \mu\text{m}$ . (b) With the y-axis presenting per cent of total spray volume, and bin sizing of  $5 \mu\text{m}$ . Sizing data taken from all valid radial locations at given height. Data processed as described in Section 2.4. See Figure 2 for measurement locations.

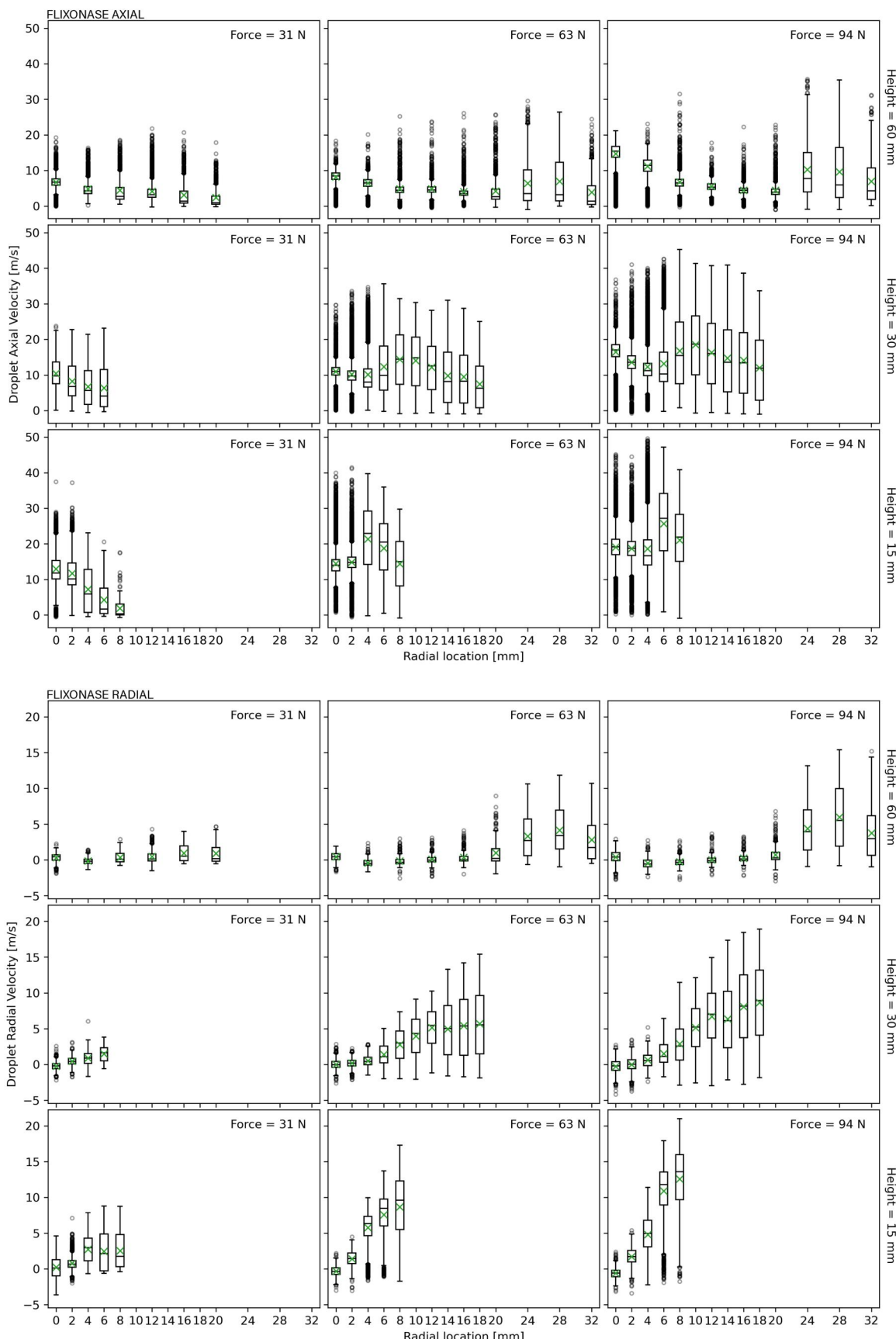


**Figure 8.** Boxplots of axial and radial velocity from Flixonase bottle at varying radial locations: See Figure 2 for velocity and measurement locations. The median is the middle horizontal line and mean is the green X, while the whiskers are values within 1.5 times the interquartile range and semi-opaque circles are outliers.

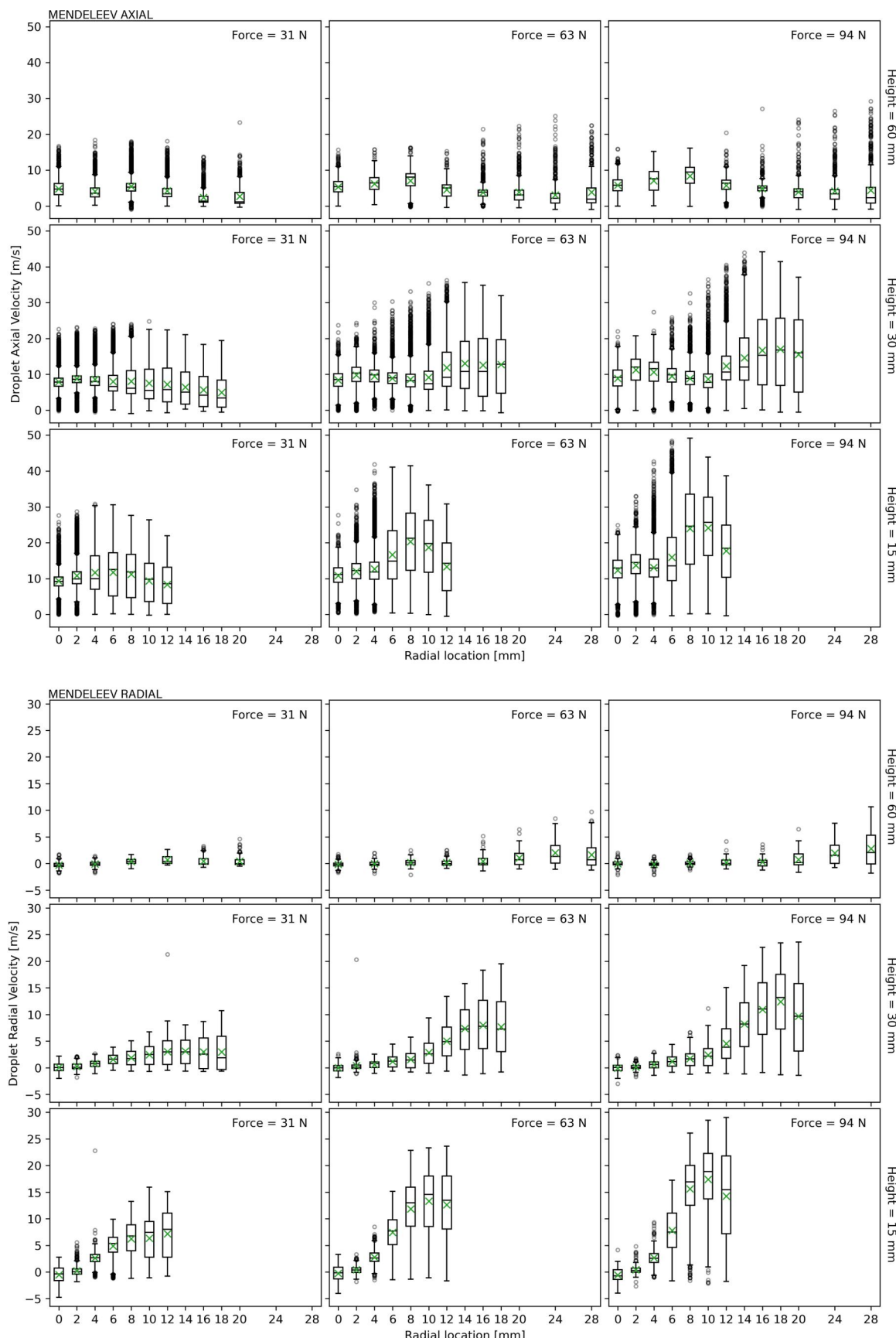


**Figure 9.** Boxplots of axial and radial velocity from Mendeleev bottle at varying radial locations. See Figure 2 for velocity and measurement locations. The median is represented by the middle horizontal line and the mean is represented by the green X. Outliers are indicated by semi-opaque circles.

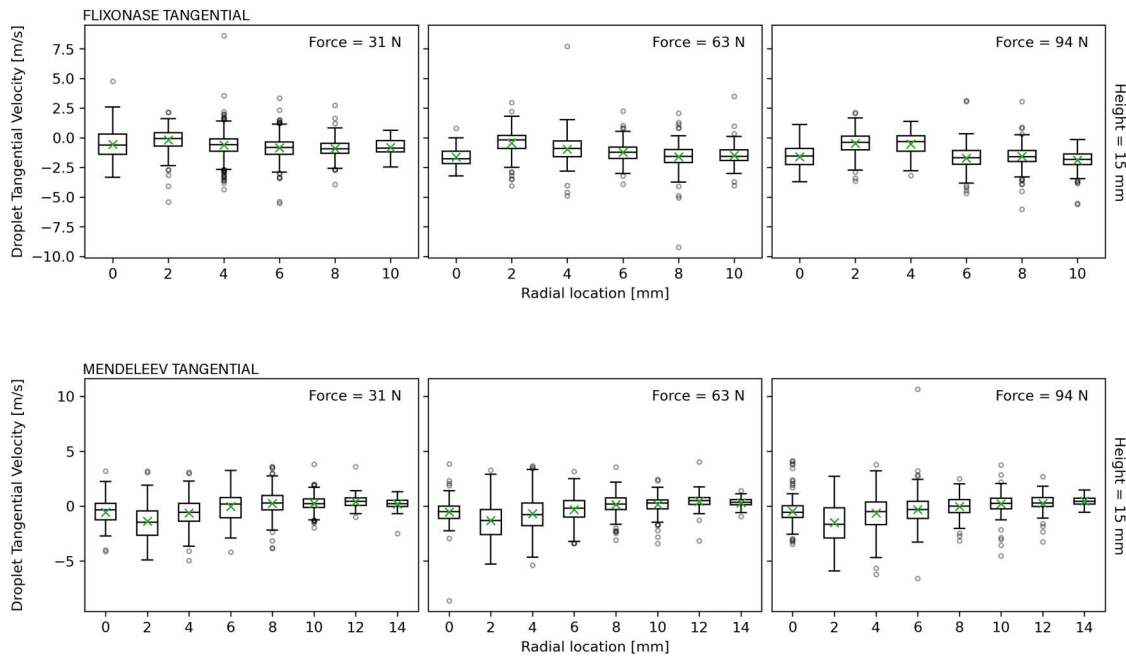


**Figure 10.** Boxplots of tangential velocity from Flixonase and Mendeleev bottles at varying radial locations and each actuation force at a height of 15 mm. See Figure 2 for velocity and measurement locations. The median is represented by the middle horizontal line and mean is represented by the green X. Outliers are indicated by semi-opaque circles.

droplet size, providing insight into droplet behavior of both variables shown in Figure 11. The results show the droplet velocity versus diameter profiles are similar between the Flixonase and Mendeleev nozzles for all heights and actuation forces.

The blue circles represent droplets measured in the center of the spray and these droplets tend to be smaller in diameter typically less than  $10 \mu\text{m}$  diameter and exhibited slower velocities approximately less than half the maximum velocity, which varied by actuation force. Droplets larger than  $10 \mu\text{m}$  diameter were found further from the centerline (black or red points), depending on the nozzle tip's spray height. The color scheme demonstrates a strong positive gradient where the larger the diameter, the greater the velocity. This gradient shows a linear relationship between axial velocity and droplet diameter, particularly when coincident with the hollow spray cone from the nozzle outlet, as the larger droplets carry more momentum and decelerate slower. The work by Liu, Doub, and Guo (2010) also found a trend of larger droplets maintaining higher velocities than smaller droplets for three nasal spray bottles they investigated, attributing this to the greater momentum of the larger droplets.

### 3.5. Ensemble scatterplots

In Figures 12 and 13 we present a novel analysis of showing the spray velocity profile over time. The axial

droplet velocities at the centerline for all spray events measured were plotted. Typically 7 sprays were overlaid, except for the Flixonase bottle at a height of 15 mm with an actuation force of 94 N having 6 sprays.

While the PDPA system can record axial velocity and droplet size simultaneously, only 15% of the data collected contained both velocity and droplet size; the remaining data provided velocity values only without diameter measurement. Figure 12 displays all measured velocity data to establish the profile with the larger data set, while 13 includes only data with both size and velocity measurements. The profiles of both figures match, despite the reduced data count.

In general, there are a greater number of larger droplets at the lower actuation force, which follows the idea that a lower actuation force produces less energy imparted on the fluid and hence less breakup of the droplets. When the actuation force increases, droplet size decreases (less bright green points), axial velocity increases and spray duration decreases.

For the Flixonase device at higher actuation force (63 N and 94 N), the profiles are relatively consistent throughout the spray event. At 31 N, and 15 mm height a distinct group of smaller slower droplets and another of faster larger droplets and their velocities persist throughout the spray event.

For the Mendeleev device, there are two distinct stages to the spray profile at higher actuation force

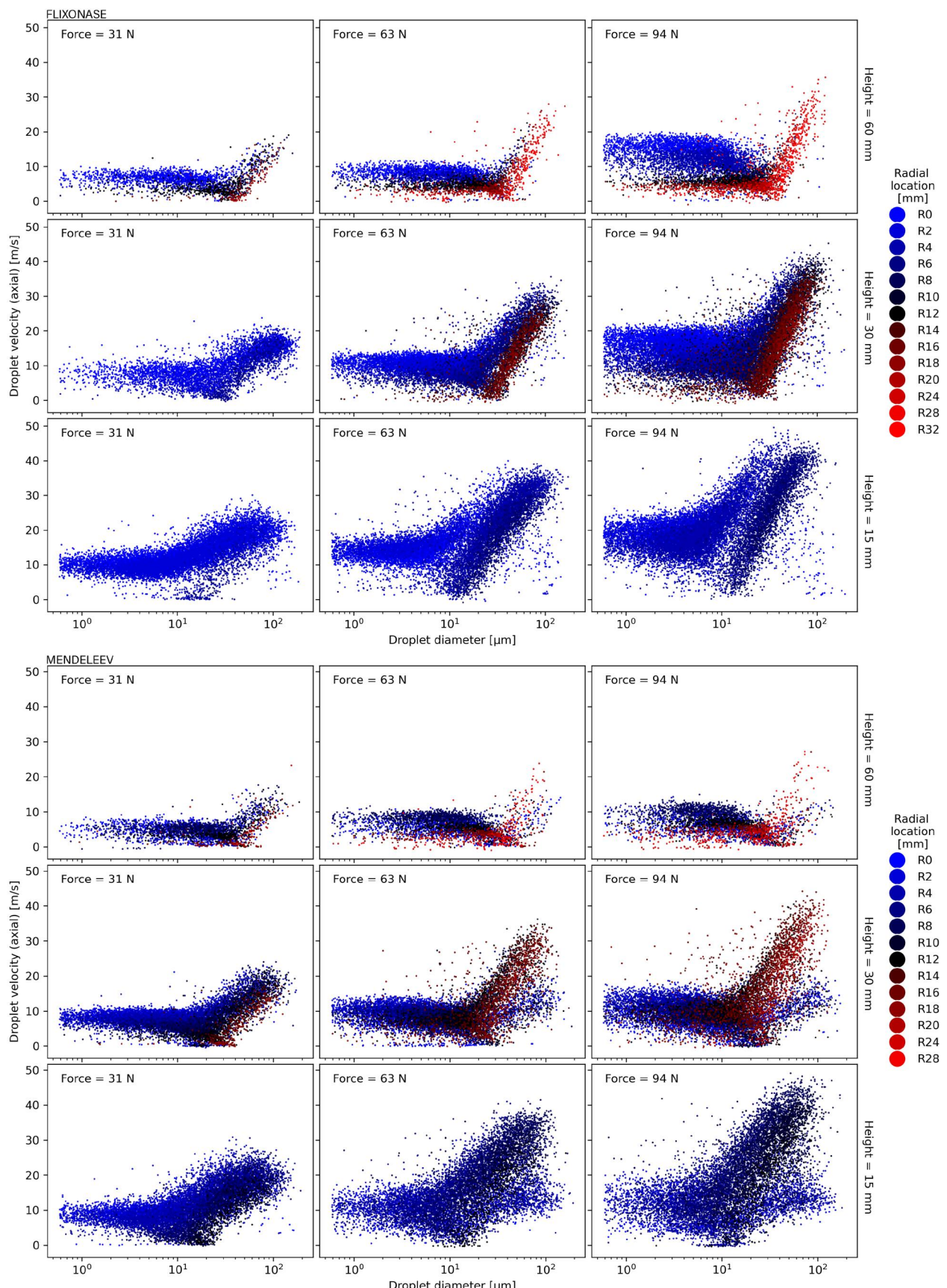


**Figure 11.** Scatterplot of axial droplet velocity vs diameter at all measured radial locations. TOP: Flixonase, BOTTOM: Mendeleev, 3x3 subplots. Columns depict actuation force and rows are height from nozzle tip. See Figure 2 for velocity and measurement locations.

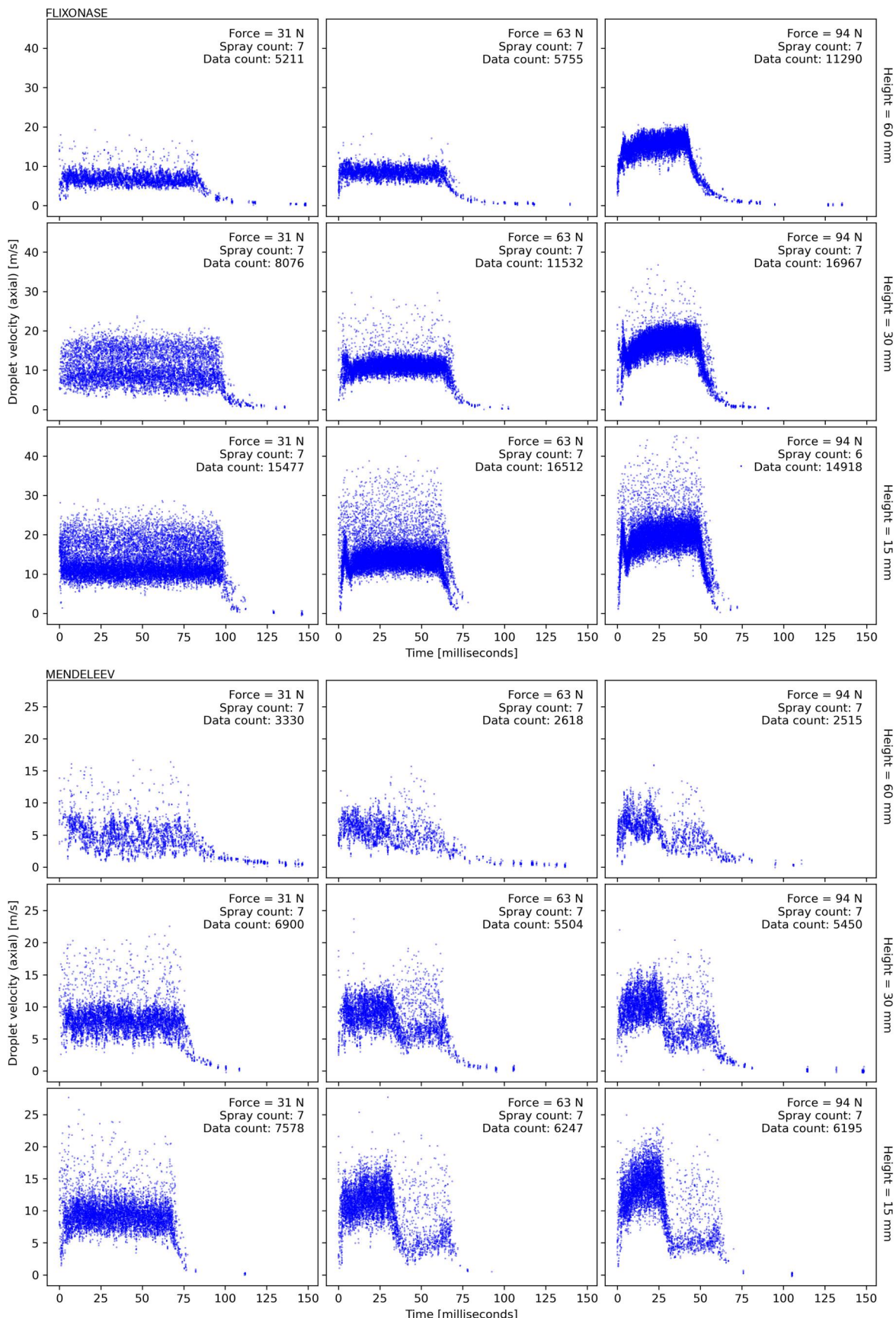


**Figure 12.** Ensemble scatterplot of axial droplet velocity over time at radial location R0. TOP: Flixonase, BOTTOM: Mendeleev, 3x3 subplots. Columns depict actuation force and rows are height from nozzle tip. Metadata are included in each subplot, where “Spray count” refers to the number of individual spray events overlayed and “data count” is the total number of data samples used. See Figure 2 for velocity and measurement locations.

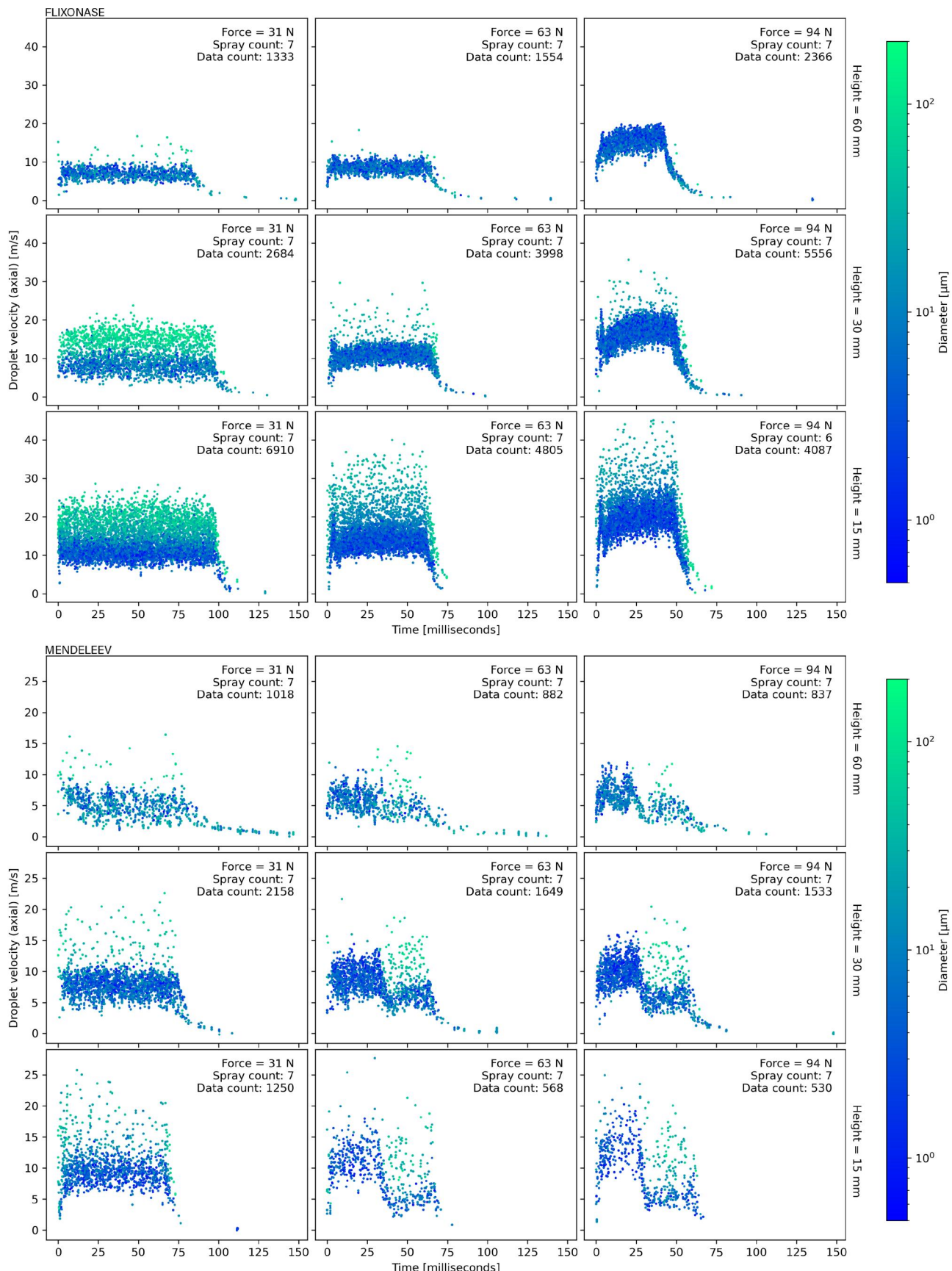


**Figure 13.** Ensemble scatterplot of axial droplet velocity over time (with color scale indicating droplet diameter) at radial location R0. TOP: Flixonase, BOTTOM: Mendeleev, 3x3 subplots. Columns depict actuation force and rows are height from nozzle tip. Metadata are included in each subplot, where “Spray count” refers to the number of individual spray events overlayed and “data count” is the total number of data samples used. See Figure 2 for velocity and measurement locations.

(63 N and 94 N). The first half produces a faster and finer spray and the second half is generally slower with a greater quantity of larger droplets. These two halves of each spray profile are relatively coincident in their timing with the delay in the spray after the actuation stroke is complete, which is discussed in the next section.

### 3.6. Delay between stroke completion and collapse of spray cone

Delay times between the end of the actuation stroke and the end of the spray (collapse of spray cone) are shown in **Table 3**. There is a negligible delay between the end-of-stroke and collapse of the spray cone for the Flixonase device at all actuation forces, and the Mendeleev at 31 N. At higher actuation forces of 63 N and 94 N, the Mendeleev device continued spraying for approximately twice as long as it took for the

**Table 3.** Tabulated results of the mean delay in milliseconds between the end of the actuation stroke and the collapse of the spray cone.

Spray device	Actuation force [N]	Mean delay [ms]	SD
Flixonase	31	0.00	0.00
	63	1.04	2.08
	94	0.00	0.00
Mendeleev	31	1.04	2.08
	63	29.17	3.40
	94	32.29	2.08

SD is the standard deviation of the data set.

actuation stroke to complete. This implies that there is stored fluid pressure within the device.

To explain the fluid pressure storage, the Mendeleev device was disassembled, as seen in **Figure 14a** showing that there is an additional mechanism in the device that is causing stored pressure and the delay between actuation and spray completion. The additional mechanism acts as a pressure buffer, smoothing the fluid pressure profile and creating a more consistent droplet size distribution. As a comparison a schematic of a more typical spray device of a fixed volume with a simple check valve, like the one found in the Flixonase bottle, is shown in **Figure 14b**.

### 3.7. Percent count vs percent volume

**Figure 15** compares data count at each measurement location and the spray volume per location. The data points vary in size to show the different percentage values.

The Mendeleev counts are distributed evenly at each height plane. This is shown by the relatively consistent sizing of the green points at each height plane. However, for the Flixonase device, there are greater differences in the size of green points at each height. There is a tendency for a greater percentage of total count of droplets toward the center of the spray. The peak count and peak volume were not necessarily found in the same location. This was most evident from the Flixonase bottle at 63 N and 94 N. While the

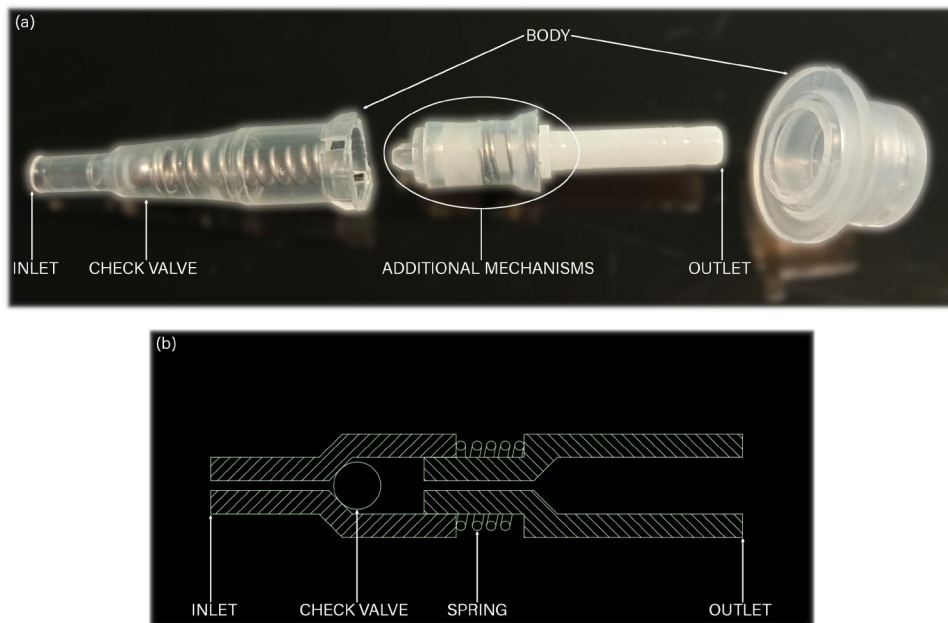


**Figure 14.** (a) The disassembled pump mechanism of the Mendeleev bottle. The “additional mechanisms” are likely a pressure buffer causing the continued spray after the completed actuation stroke. (b) A cross-sectional schematic view of a more typical nasal spray pump mechanism used in the Flixonase nozzle.

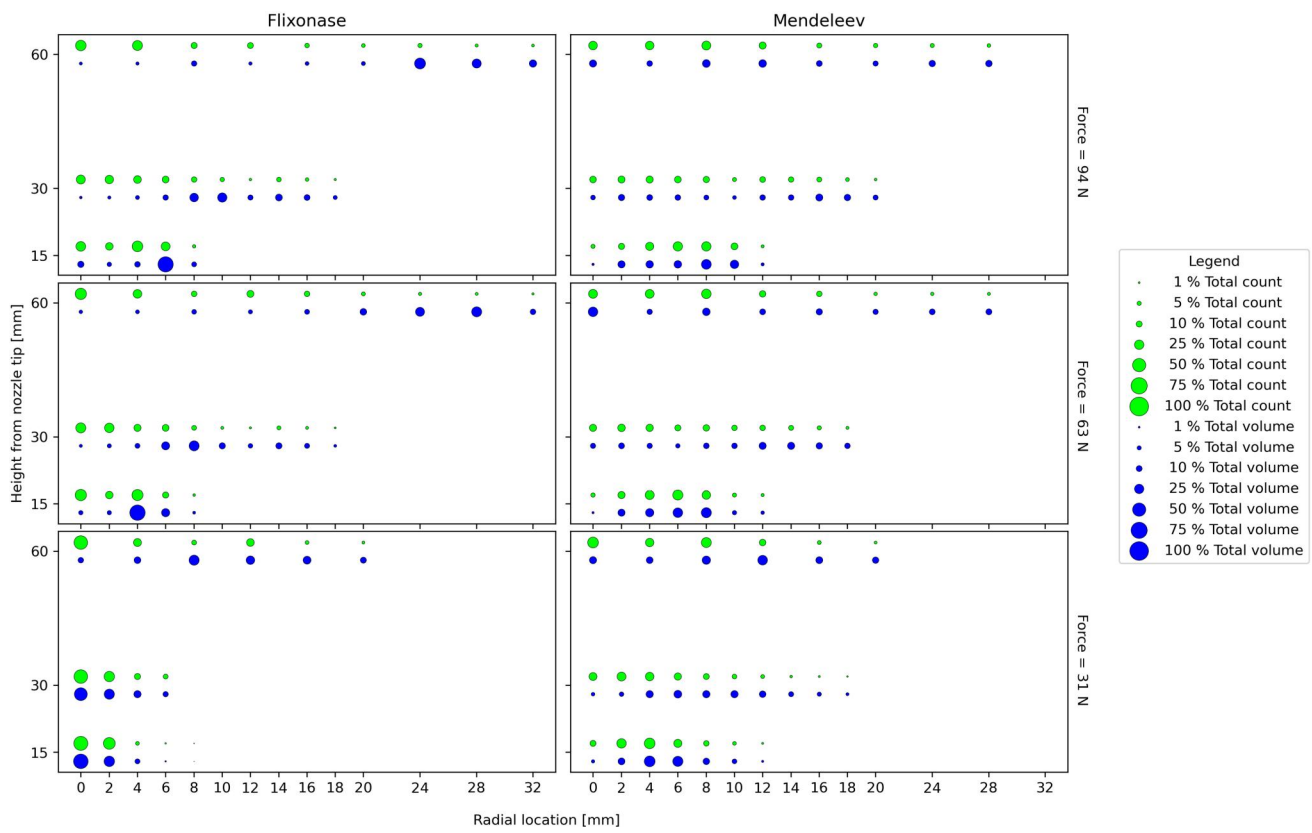


**Figure 15.** Comparison between axial velocity data count and volume fraction at each measurement location. Green points represent the percentage of total count while the blue points represents the percentage of spray volume. Each row of points will add up to 100%. See Figure 2 for measurement locations.

highest count tended toward the center (larger green dots), the peak percent of the volume was toward the outer edge of the spray (larger blue dots). Larger droplets will tend to maintain their velocity in a direction coincident with the hollow cone sheet due to their higher mass. The liquid spray causes eddies within the surrounding air. These eddies are particularly strong within the spray cone, as it is surrounded by the influence of the fluid. Smaller droplets are more influenced by the eddies and so these eddies will cause fluctuations of the particle from its initial location along the hollow cone sheet toward the spray center.

### 3.8. General velocity characterisation

Liu, Doub, and Guo (2010) found that the velocity characteristics of nasal sprays can be derived by measuring on the centerline of the spray. We agree with this conclusion as a general, rule-of-thumb type of velocity measurement but it may be inadequate to fully describe the spray behavior when considering mass fraction. The bulk of the total spray mass typically coincides with the hollow cone sheet at the higher actuation force (representing an adult actuation). For

example, in Figure 15, the Flixonase device at 63 N close to the nozzle (15 mm height) exhibited the largest portion of fluid mass at the radial location of 4 mm. The mean axial and radial velocities at this location were 21.4 m/s and 5.8 m/s, respectively. The axial and radial velocity components combine for a resulting mean velocity of 22.2 m/s. At the same height, the axial velocity at the centerline of the spray was 14.5 m/s, 35% less than the velocity at the location with the highest mass fraction.

Both Liu, Doub, and Guo (2010) and the present study used water as the fluid in the nasal spray investigations. This investigation found that smaller droplets were predominant in the spray center. Drug formulations typically have a higher viscosity than water that would reduce the number of smaller droplets. The data sample for velocity measurements of drug formulations on the centerline may be reduced by the fewer smaller droplets.

The experimental technique and analysis demonstrated in this paper have shown the potential for characterizing nasal spray droplet size and three-dimensional velocity behavior throughout the spray plume. The following steps would build on this work.

Use of a ballscrew type positioning system with finely marked graduations would provide greater positional accuracy. An automated CNC system in addition to this would increase the efficiency of the experimental process.

Take measurements in multiple directions from the concentric axis to allow for asymmetrical sprays.

#### 4. Conclusion

This paper presented a new method to characterize nasal spray droplet size and three-dimensional velocity behavior throughout the spray plume. A three-channel PDPA system was used to measure the size and velocity of water droplets from two commercially available nasal spray devices. Both of these devices utilize the pressure-swirl nozzle. One nasal spray device had a typical fixed-volume type pump which ejected fluid only during actuation. The other nasal spray pump included a pressure buffering device, which stored fluid pressure during actuation and released the pressure after the actuation stroke was completed. An in-house automated pneumatic actuation device was used to repeatedly actuate the nasal sprays at the average child, average adult and maximum adult forces. The works herein drew the following conclusions.

Larger, faster droplets were found near the spray periphery, as the higher droplet momentum kept them coincident with the hollow cone sheet that formed from the orifice exit of the pressure-swirl atomisers.

Smaller and slower droplets tended to makeup the core of the spray, as they were strongly influenced by air movement. It is presumed that the spray plume formed eddies in the air, causing the smaller droplets to move towards the spray centre through random motion and flow entrainment, rather than stay coincident with the hollow cone sheet. The higher viscosity of drug formulations may prevent these smaller droplets from forming.

Measuring velocity at the centrelne may be inadequate to characterise velocity behaviour of nasal sprays when considering radial velocity and mass fraction. As nasal sprays tend to have increased viscosity, the number count of smaller droplets within the spray centre may decrease, reducing the validity of measurements at the centre.

Axial velocity was the dominant component of droplet velocity.

Radial velocity was negligible near the spray centre but significant near the spray's edge (a result of the cone shape of the spray).

Tangential velocity was non-zero but negligible throughout and was likely caused by random air movement.

Fluid pressure buffer systems can reduce the influence of actuation force on droplet size distribution, keeping a more consistent DSD at increased actuation forces.

In line with existing literature, an increase in actuation force causes an increase in droplet velocity and a decrease in droplet sizing.

#### Nomenclature

$D_{32}$	Sauter mean diameter
DSD	droplet size distribution
PDPA	phase Doppler particle analysis
PIV	particle image velocimetry
SMD	Sauter mean diameter

#### Acknowledgements

The authors would like to thank Deakin University for the PhD scholarship and start-up funds to support this project.

#### Disclosure statement

The authors declare that they have no potential conflicts of interest.

#### ORCID

James Van Strien  <http://orcid.org/0000-0002-5258-8892>  
Kiao Inthavong  <http://orcid.org/0000-0003-0476-0237>

#### References

- Belhade, A., A. Vallet, M. Amielh, and F. Anselmet. 2012. Pressure-swirl atomization: Modeling and experimental approaches. *Int. J. Multiphase Flow*. 39:13–20. doi: [10.1016/j.ijmultiphaseflow.2011.09.009](https://doi.org/10.1016/j.ijmultiphaseflow.2011.09.009).
- Dafsari, R. A., F. Vashahi, and J. Lee. 2017. Effect of swirl chamber length on the atomization characteristics of a pressure-swirl nozzle. *Atomiz. Spr.* 27 (10):859–74. doi: [10.1615/AtomizSpr.2017024777](https://doi.org/10.1615/AtomizSpr.2017024777).
- Dafsari, R. A., H. J. Lee, J. Han, and J. Lee. 2019a. Evaluation of the atomization characteristics of aviation fuels with different viscosities using a pressure swirl atomizer. *Int. J. Heat Mass Transf.* 145:118704. doi: [10.1016/j.ijheatmasstransfer.2019.118704](https://doi.org/10.1016/j.ijheatmasstransfer.2019.118704).
- Dafsari, R. A., H. J. Lee, J. Han, D.-C. Park, and J. Lee. 2019b. Viscosity effect on the pressure swirl atomization of an alternative aviation fuel. *Fuel*. 240:179–91. doi: [10.1016/j.fuel.2018.11.132](https://doi.org/10.1016/j.fuel.2018.11.132).
- Dayal, P., M. Sudhan Shaik, and M. Singh. 2004. Evaluation of different parameters that affect droplet-size distribution from nasal sprays using the Malvern Spraytec. *J. Pharm. Sci.* 93 (7):1725–42. doi: [10.1002/jps.20090](https://doi.org/10.1002/jps.20090).
- Dorfner, V., J. Domnick, F. Durst, and R. Kohler. 1995. Viscosity and surface tension effects in pressure swirl atomization. *Atomiz. Spr.* 5 (3):261–85. doi: [10.1615/AtomizSpr.v5.i3.20](https://doi.org/10.1615/AtomizSpr.v5.i3.20).

- Doughty, D. V., C. Vibbert, A. Kewalramani, M. E. Bollinger, and R. N. Dalby. 2011. Automated actuation of nasal spray products: Determination and comparison of adult and pediatric settings. *Drug Dev. Ind. Pharm.* 37 (3):359–66. doi: [10.3109/03639045.2010.520321](https://doi.org/10.3109/03639045.2010.520321).
- Durdina, L., J. Jedelsky, and M. Jicha. 2012. Spray structure of a pressure-swirl atomizer for combustion applications. In *EPJ web of conferences*, Vol. 25, 01010. Les Ulis, France: EDP Sciences. doi: [10.1051/epjconf/20122501010](https://doi.org/10.1051/epjconf/20122501010).
- Durdina, L., J. Jedelsky, and M. Jicha. 2014. Investigation and comparison of spray characteristics of pressure-swirl atomizers for a small-sized aircraft turbine engine. *Int. J. Heat Mass Transf.* 78:892–900. doi: [10.1016/j.ijheatmasstransfer.2014.07.066](https://doi.org/10.1016/j.ijheatmasstransfer.2014.07.066).
- Fung, M. C., K. Inthavong, W. Yang, P. Lappas, and J. Tu. 2013. External characteristics of unsteady spray atomization from a nasal spray device. *J. Pharm. Sci.* 102 (3): 1024–35. doi: [10.1002/jps.23449](https://doi.org/10.1002/jps.23449).
- Gao, M., X. Shen, and S. Mao. 2020. Factors influencing drug deposition in the nasal cavity upon delivery via nasal sprays. *J. Pharm. Investig.* 50 (3):251–9. doi: [10.1007/s40005-020-00482-z](https://doi.org/10.1007/s40005-020-00482-z).
- Guo, C., K. J. Stine, J. F. Kauffman, and W. H. Doub. 2008. Assessment of the influence factors on in vitro testing of nasal sprays using Box-Behnken experimental design. *Eur. J. Pharm. Sci.* 35 (5):417–26. doi: [10.1016/j.ejpharm.2008.09.001](https://doi.org/10.1016/j.ejpharm.2008.09.001).
- Hansen, K. G., J. Madsen, C. M. Trinh, C. H. Ibsen, T. Solberg, and B. H. Hjertager. 2002. A computational and experimental study of the internal flow in a scaled pressure-swirl atomizer. *Zaragoza*. 9:11.
- Hosseini, S., X. Wei, J. V. Wilkins, Jr, C. P. Ferguson, R. Mohammadi, G. Vorona, and L. Golshahi. 2019. In vitro measurement of regional nasal drug delivery with Flonase®, Flonase® Sensimist,™ and MAD Nasal™ in anatomically correct nasal airway replicas of pediatric and adult human subjects. *J. Aerosol Med. Pulm. Drug Deliv.* 32 (6):374–85. doi: [10.1089/jamp.2019.1523](https://doi.org/10.1089/jamp.2019.1523).
- Inthavong, K., M. C. Fung, W. Yang, and J. Tu. 2015. Measurements of droplet size distribution and analysis of nasal spray atomization from different actuation pressure. *J. Aerosol Med. Pulm. Drug Deliv.* 28 (1):59–67. doi: [10.1089/jamp.2013.1093](https://doi.org/10.1089/jamp.2013.1093).
- Inthavong, K., M. C. Fung, X. Tong, W. Yang, and J. Tu. 2014. High resolution visualization and analysis of nasal spray drug delivery. *Pharm. Res.* 31 (8):1930–7. doi: [10.1007/s11095-013-1294-y](https://doi.org/10.1007/s11095-013-1294-y).
- Inthavong, K., W. Yang, M. C. Fung, and J. Y. Tu. 2012. External and near-nozzle spray characteristics of a continuous spray atomized from a nasal spray device. *Aerosol Sci. Technol.* 46 (2):165–77. doi: [10.1080/02786826.2011.617793](https://doi.org/10.1080/02786826.2011.617793).
- Inthavong, K., Z. F. Tian, H. F. Li, J. Y. Tu, W. Yang, C. L. Xue, and C. G. Li. 2006. A numerical study of spray particle deposition in a human nasal cavity. *Aerosol Sci. Technol.* 40 (11):1034–45. doi: [10.1080/02786820600924978](https://doi.org/10.1080/02786820600924978).
- Kimbell, J. S., R. A. Segal, B. Asgharian, B. A. Wong, J. D. Schroeter, J. P. Southall, C. J. Dickens, G. Brace, and F. J. Miller. 2007. Characterization of deposition from nasal spray devices using a computational fluid dynamics model of the human nasal passages. *J. Aerosol Med.* 20 (1):59–74. doi: [10.1089/jam.2006.0531](https://doi.org/10.1089/jam.2006.0531).
- Kowalcuk, P. B., and J. Drzymala. 2016. Physical meaning of the Sauter mean diameter of spherical particulate matter. *Part. Sci. Technol.* 34 (6):645–7. doi: [10.1080/02726351.2015.1099582](https://doi.org/10.1080/02726351.2015.1099582).
- Lefebvre, A. H., and V. G. McDonell. 2017. *Atomization and sprays*. Boca Raton, FL: CRC Press.
- Liu, X., W. H. Doub, and C. Guo. 2010. Evaluation of droplet velocity and size from nasal spray devices using phase Doppler anemometry (PDA). *Int. J. Pharm.* 388 (1–2): 82–7. doi: [10.1016/j.ijpharm.2009.12.041](https://doi.org/10.1016/j.ijpharm.2009.12.041).
- Liu, X., W. H. Doub, and C. Guo. 2011. Assessment of the influence factors on nasal spray droplet velocity using Phase-Doppler Anemometry (PDA). *AAPS PharmSciTech.* 12 (1):337–43. doi: [10.1208/s12249-011-9594-1](https://doi.org/10.1208/s12249-011-9594-1).
- Sijs, R., S. Kooij, H. J. Holterman, J. Van De Zande, and D. Bonn. 2021. Drop size measurement techniques for sprays: Comparison of image analysis, phase Doppler particle analysis, and laser diffraction. *AIP Adv.* 11 (1): 015315. doi: [10.1063/5.0018667](https://doi.org/10.1063/5.0018667).
- Sumer, B., N. Erkan, O. Uzol, and I. H. Tuncer. 2012. Experimental and numerical investigation of a pressure swirl atomizer. Proceedings of the ICLASS, Heidelberg, Germany, 2–6.
- Sun, Y., A. M. Alkhedhair, Z. Guan, and K. Hooman. 2018. Numerical and experimental study on the spray characteristics of full-cone pressure swirl atomizers. *Energy*. 160:678–92. doi: [10.1016/j.energy.2018.07.060](https://doi.org/10.1016/j.energy.2018.07.060).
- Tratnig, A., and G. Brenn. 2010. Drop size spectra in sprays from pressure-swirl atomizers. *Int. J. Multiphase Flow*. 36 (5):349–63. doi: [10.1016/j.ijmultiphaseflow.2010.01.008](https://doi.org/10.1016/j.ijmultiphaseflow.2010.01.008).
- Van Strien, J., P. Petersen, P. Lappas, L. Yeo, A. Rezk, S. Vahaji, and K. Inthavong. 2022. Spray characteristics from nasal spray atomization. *J. Aerosol Sci.* 165:106009. doi: [10.1016/j.jaerosci.2022.106009](https://doi.org/10.1016/j.jaerosci.2022.106009).
- Williams, T. J., J. C. Gilles, and S. Murphy. 2009. Velocity profiling of sprays from pharmaceutical nasal spray pumps. *Respiratory Drug Delivery Europe*. 441–4.
- Zhao, J., and L. Yang. 2012. Simulation and experimental study on the atomization character of the pressure-swirl nozzle. *OJFD*. 02 (04):271–7. doi: [10.4236/ojfd.2012.24A032](https://doi.org/10.4236/ojfd.2012.24A032).